Radioactive Source Detection by Sensor Networks

Sean M. Brennan, Angela M. Mielke, and David C. Torney

***Abstract*—Detection limits of sensor networks for moving radioactive sources are characterized, using Bayesian methods in conjunction with computer simulation. These studies involve point sources moving at constant velocity, emulating vehicular conveyance on a straight road. For networks involving ten nodes, respective Bayesian methods are implementable in real time. We probe the increased computational requirements incurred by larger numbers of nodes and source trajectory parameters. The complexity appears quadratic in the number of nodes and, also, numerous trajectory parameters may be used. We investigate the consequences of different levels of background radiation. Simulations are shown to be useful for ranking candidate node layouts. We study the detection capabilities of individual sensors and the scalability of detection with sensor density; near the detection limit, increasing the number of sensors can accrue subproportional network sensitivity.**

***Index Terms*—Distributed sensor network, gamma radiation, Geiger–Müller counter, Monte Carlo integration, Poisson statistics, true negative, true positive.**

I. Introduction

CONSUMMATE detection of nuclear materials transport is a homeland security desideratum [1]. Portal monitoring is the respective state of the art, but in the future, distributed sensor networks (DSNs) could provide wider surveillance capabilities[2].

As will be seen, our methods for radioactive source detection are elaborations upon those yielding estimates of source parameters [3], i.e., tackling an inverse problem [4]. Herein, network nodes are stationary and the source is mobile. The nodes are equipped with a radiation sensor which records counts – such as a Geiger–Müller counter. For detection, one could implement a (background dependent) threshold on the summed counts [3], [5], but for this approach to be effective, the source's trajectory must, in essence, be known, and here we explore more general methods, effective for considerable "universes" of possible trajectories.

Herein, *signal* refers to counts derived from the source, whereas the remainder derive from *background*. Both components are assumed to obey Poisson statistics. Our models pertain to gamma sources, e.g., the "$1/r^2$ falloff" of signal. Given a network of sensors and their sensor data, comprising background plus signal, which methods afford ultimate sensitivity of detection?

Manuscript received November 30, 2004; revised February 16, 2005. This work was supported by a National Nuclear Security Administration Grant, "Distributed Sensor Networks with Collective Computation," and the University of California, operator of the Los Alamos National Laboratory under Contract W-7405-ENG-36 with the U.S. Department of Energy.

The authors are with the ISR and Theoretical Divisions, Los Alamos National Laboratory, Los Alamos, NM 87545 USA (e-mail: brennan@lanl.gov; amielke@lanl.gov; dtorney@lanl.gov).

Digital Object Identifier 10.1109/TNS.2005.850487

Bayesian methods constitute optimal, data-based inference within a prespecified universe of scenarios [6]. We describe the implementation of these methods for radioactive source detection, with scenarios comprising various source amplitudes and trajectories.

The present aims are elemental. This manuscript provides preliminary insights into the envelope of effectiveness of Bayesian detection versus its computational requirements for networks with 10–320 nodes deployed within a length of roadway: a simple model with practical ramifications [1], [5]. Bayesian methods for source parameter estimation exhibited a computational complexity exponential in the number of parameters estimated [3], limiting their implementability and fostering concerns that their specialization for detection might also be too computationally intensive to ever be useful. We establish herein that, for detection, their domain of effectiveness should include complicated, realistic models.

II. Methods

A. Overview of Bayesian Classification Methodology

The foundation for Bayesian methods is a parameterized formula for the probability of the data: $\Pr(\text{data})$ [6]. Here, parameters specify a source's amplitude and trajectory; formulation of the probability of sensor data is straightforward, as will be seen [*viz* (1) and (2)].

Here, the classes constitute a partition of "parameter space." Furthermore, there are two natural classes: either a radioactive source is or is not incident on a specified domain during a given time interval.

The probability the data originate from class c, denoted P_c; $c = 1, 2$, ensues from integrals, I_c, of $\Pr(\text{data})$ over the respective part of parameter space – with appropriate parameter weights (multiplicative factors): the renowned "prior probabilities," often assumed constant within the classes. Bayes' rule [*viz* (4)] asserts P_c equals the quotient of I_c by the sum of the I_c's.

We adopt a natural classification rule: Infer the class with maximum P_c, and if there is a tie, then infer one of the classes with maximum P_c uniformly at random. Thus, for given count data, if the integral I_c, over the class of "incident sources" exceeds that for "nonincident sources," then the underlying event is classed as incident and *vice versa*.

B. $\Pr(\text{data})$

Let x and y denote the initial coordinates of the source, and let it have amplitude a and a speed v in the positive x direction. The parameter a is the expected "counts" (dimensioned $\mathrm{m^2 s^{-1}}$). For example, a sensor at distance d meters from the source, has an expected rate of signal acquisition equal a/d^2 per second. Thus, a embodies characteristics both of the source and of the sensor. The counts recorded at a stationary node at position (x_s,

0018-9499/$20.00 © 2005 IEEE

y_s), over the interval $[0, t]$, are taken to be Poisson distributed with mean

$$\mu_s = bt + \frac{a}{|y - y_s|v} \times \left\{ \tan^{-1}\left(\frac{x - x_s + vt}{|y - y_s|}\right) - \tan^{-1}\left(\frac{x - x_s}{|y - y_s|}\right)\right\} \quad (1)$$

where b (dimensioned s^{-1}) denotes the expected background rate. [(1) follows from (7), derived in the Appendix.] For simplicity, b is assumed to be the same for all sensors [5].

Thus, if a sensor with expected number of counts μ_s records k counts, then the corresponding (Poisson) probability of these data equals

$$\exp\{-\mu_s\}\frac{\mu_s^k}{k!}.$$

The product of such "Poisson factors" for all the sensors and for time intervals with available data constitutes the requisite formula for the probability of the data, a function of parameters a, v, x and y

$$\Pr(\text{data}) = \prod_{s=1}^{S}\prod_{\tau=1}^{T}\exp\{-\mu_{s\tau}\}\frac{\mu_{s\tau}^{k_{s\tau}}}{k_{s\tau}!} \quad (2)$$

where S is the number of nodes and T the number of time intervals over which signals have been collected and where $k_{s\tau}$ denotes the number of counts recorded at node s over interval τ, given the respective expected value $\mu_{s\tau}$.

The probability that the data originate from class c is proportional to an integral of $\Pr(\text{data})$

$$I_c = \frac{1}{|V_c|}\int_{V_c}\Pr(\text{data})\,d\pi;\ c = 1, 2 \quad (3)$$

where π denotes the parameters (a, v, x and y); where V_c is the portion of parameter space constituting class c; and where the respective volume is denoted $|V_c|$; $c = 1, 2$. Equation (3) contains no π-dependent factor; thus, prior probabilities are assumed constant within the classes.

C. Infrastructure

It is apparent that, in general, (3) must be evaluated numerically—as is the norm for Bayesian statistics [7]. Even if statistical fluctuations were negligible and even for $S = 1$, integrals over level sets of (1) would pose a challenge for analytic evaluation. For the present objectives, both the large "dynamic range" of the integrands and the modest dimensionality (the number of parameters) commend Monte Carlo (sampling) methods over standard numerical quadrature methods [8, Ch. 4].

Because of the constant prior probabilities, I_c was approximated by uniform sampling of V_c: the sum of the integrands at the sampled points divided by the number of sampled points converges to I_c, given by (3) [8], [9]. Furthermore, to forestall underflow and overflow, with each succeeding point, the logarithm of the partial sum was employed and appropriately incremented.

We implemented (3) for our two classes. Thus, with equal prior probabilities of belonging to each class, the probability P_c, of belonging to class c given count data $k_{11}, k_{12}, \ldots, k_{ST}$, equals

$$P_c = \frac{I_c}{I_1 + I_2},\ \ c = 1, 2. \quad (4)$$

Note that the form of (4) enables omission of the factorials originating from (2).

Therefore, we uniformly sampled from V_c; $c = 1, 2$, yielding source trajectories and amplitudes. For each source, we used (1) to obtain the respective $\mu_{s\tau}$; $s = 1, 2, \ldots, S$, $\tau = 1, 2, \ldots, T$, and $k_{s\tau}$ was then obtained by sampling a Poisson distribution with mean $\mu_{s\tau}$ [10, Poisson-random-variable generation]. Next, (4) was evaluated, using (3), and, essentially, the proportion of times $I_c > I_{c'}$ recorded ($c \neq c'$) to obtain the estimate for the correct classification rate. (We will shortly say more about our treatment of "$I_c = I_{c'}$".) One thousand trials were typically implemented, for both classes, to obtain the rates given in the results. For the first class of incident trajectories, the correct classification rate is called the true positive (TP) rate, and for the second class, this rate is called the true negative (TN) rate.

When $I_c \doteq I_{c'}$, i.e., the magnitude of the relative difference of their logarithms was sufficiently small – not exceeding a cutoff Ξ in magnitude – the respective count of correct classification was incremented by 1/2. We introduced Ξ because, otherwise, near the detection limit, the TP rate sometimes fell to the vicinity of 0.4 (returning to 0.5 with smaller a). With our current aims, such presumably artifactual behavior was a distraction, and it was quashed by using $\Xi = 10^{-4}$ for incident trajectories and $\Xi = 10^{-5}$ for nonincident trajectories. Unless otherwise specified, these values of Ξ were used. For correct classification rates greater than 0.6, such Ξ's had negligible effect.

TABLE I
RATES OF "GETTING IT RIGHT" (TP, TN) FOR SOURCES OF DIFFERING AMPLITUDES, AND BACKGROUNDS, USING DATA FROM 32 SENSORS, RANDOMLY PLACED IN THE ROADWAY, WITH THE SAME CONFIGURATION IN ALL CASES. THE ROW FOR $b = 10$ IS REPRODUCED FROM TABLE II. 1,000 DIFFERENT, UNIFORMLY DISTRIBUTED TRAJECTORIES (OF EACH CLASS) WERE SIMULATED AND THE MAXIMUM I_c WAS USED TO PREDICT THE CLASS. FOR THE CASES WITH $b = 1$, THE $\Xi = 10^{-3}$, MODESTLY DIMINISHING THE $a = 10$ TN RATE FROM WHAT IT WOULD HAVE BEEN FOR THE DEFAULT VALUES OF Ξ

$a =$	1	10	100	1000
$b = 1$ TP	0.54	0.79	–	–
$b = 1$ TN	0.50	0.84	–	–
$b = 10$ TP	0.52	0.68	0.99	–
$b = 10$ TN	0.50	0.89	1.00	–
$b = 100$ TP	–	0.52	0.71	0.99
$b = 100$ TN	–	0.50	0.50	1.00

D. Simulations

Our simulations abstractly model the transport of radioactive sources in vehicles moving on straight roadways by means of constant velocity sources. Speeds v, between 10 m/s and 30 m/s were taken to be equally probable. Source amplitudes ranged between 10^{-1} and 10^{3}. Background radiation was usually taken to have a (relatively high) expected value of 10 [3], a small enough value so that statistical fluctuations (and discreteness of the counts) influenced our results [*viz* Table I]. Data were collected for 20 consecutive time intervals, i.e., $T = 20$, each of 1 s duration.

The segment of roadway "under surveillance" was taken to be a rectangle with a width 10 m and length 600 m. The x coordinate was parallel to long axis, and the y coordinate the short axis. (For simplicity, all "z coordinates" were assumed equal to zero.)

Thus, the first class consisted of all trajectories incident on this rectangle: events one wishes to detect. In detail, centering the rectangle on the origin, a source of velocity with magnitude v had its initial x coordinate uniform over $[-10v - 300, 300 - 10v]$ and its y coordinate uniform over $[-5, 5]$. Such trajectories locate the source within the 10 m by 600 m rectangle for at least half of the 20 s of data collection. Thus, V_1 is a prismatic portion of parameter space, coordinatized by x, y and v, falling in dependent intervals $[-10v - 300, 300 - 10v]$, $[-5, 5]$ and [10, 30], respectively.

The second class consisted of parameters for 20-s long trajectories intersecting a square, centered about the rectangle, with sides two orders of magnitude larger than the circumference thereof – excluding the trajectories of the first class. We could have chosen effectively infinitely distant trajectories to constitute this class, with background radiation alone yielding the count data, but our choice profitably anticipates real-world ambiguities because sources in V_2 "near" V_1 mimic the latter's.

For these sources, using from 10^4 to 10^5 points to compute the I_c's effectively suppressed fluctuations in estimates of the TP and TN rates. A suitable number of points appeared to be largely dependent on the number of nodes, with $p = 10^4$ appropriate for simulations involving ten nodes and $p = 10^5$ for simulations involving 100 nodes. As the number of nodes increases, a greater variety of trajectories must be simulated to effectively circumscribe the trajectories' data signatures. Fixing the number of nodes, with a did not influence the effectual number of sampled points.

To foster some insights into these key infrastructural components of our methodology, we provide the results from simulations of 100 incident and nonincident trajectories with 32 randomly placed nodes and with $a = 10$ (yielding a detectable signal). p ranged up to 320 000. Fig. 1 depicts the averages, over trajectories, of

$$\frac{\log\left(\frac{I_1(p)}{I_2(p)}\right)}{\log\left(\frac{I_1(320\,000)}{I_2(320\,000)}\right)}.$$

The "half-numbers" for convergence are approximately $p = 100\,000$ and $p = 20\,000$, for incident and nonincident trajectories, respectively, implying that our main simulation results, the rates appearing in the $S = 32$ ($p = 32\,000$) data of Table II, could manifest residual noise. The averages of $\log I_1(320\,000)$ were proportional to 8952.9 and 8365.5, and the averages of $\log I_2(320\,000)$ were proportional to 8584.5 and 8365.9, respectively. [Recall that (4) allowed omission of factorials from Poisson coefficients.]

Thus, in summary, because the basic formulae, such as (3), are linear in the number of nodes, S, the computational complexity of our detection algorithm is approximately S^2.

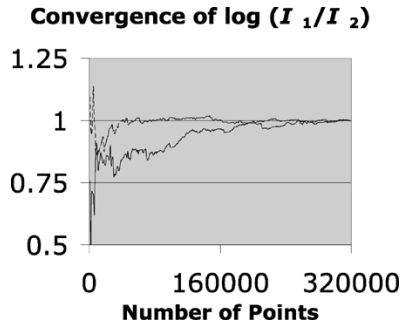

Fig. 1. Convergence of $\log(I_1/I_2)$. Abscissa: $1000 \leq p \leq 320\,000$. Ordinate: $\langle(\log(I_1(p)/I_2(p)))/(\log(I_1(320\,000)/I_2(320\,000)))\rangle$; the average is over 100, uniformly sampled trajectories. The top curve is derived from nonincident trajectories; the bottom curve is derived from incident trajectories.

TABLE II
RATES OF "GETTING IT RIGHT" (TP, TN) FOR SOURCES OF AMPLITUDES 0.1 THROUGH 1000 AND FOR 10, 32, 100, OR 320 NODES, UNIFORMLY DISTRIBUTED AT RANDOM. TO FACILITATE COMPARISON, THE SAME CONFIGURATION WAS USED FOR ALL SIMULATIONS WITH THE SAME NUMBER OF NODES. FOR A GIVEN NODE CONFIGURATION, 1000 DIFFERENT, UNIFORMLY DISTRIBUTED TRAJECTORIES (OF EACH CLASS) WERE SIMULATED AND THE MAXIMUM I_c'S USED TO PREDICT THE CLASS, USING THE Ξ'S OF THE METHODS

S	$a =$	0.1	.3125	1.0	3.125	10.0	31.25	100.0	312.5	1000.
10	TP	–	–	0.51	0.52	0.58	0.57	0.83	0.99	1.00
10	TN	–	–	0.53	0.71	0.82	0.89	0.96	1.00	1.00
32	TP	–	0.50	0.52	0.56	0.68	0.82	0.99	1.00	–
32	TN	–	0.50	0.50	0.72	0.89	0.98	1.00	1.00	–
100	TP	0.50	0.52	0.54	0.62	0.83	0.99	1.00	–	–
100	TN	0.50	0.50	0.50	0.72	0.96	1.00	1.00	–	–
320	TP	–	–	0.58	0.75	0.97	–	–	–	–
320	TN	–	–	0.50	0.78	1.00	–	–	–	–

The runtime for suitable analysis of 20 seconds' worth of data simulated for ten nodes, sampling 10^4 points to compute I_1 and I_2, was approximately 5 s on a 2.2-GHz processor.

III. RESULTS

A. Domain of Surveillance of Individual Sensors

The main motivation for this manuscript is to reveal the dependences of a DSN's radioactive source detection capabilities upon its node configuration. Therefore, as prologue, we investigate the detection capabilities of an individual sensor, simplified to the characterization of the domain surrounding the source within which a stationary sensor receives an above-cutoff expected signal from a constant velocity radioactive source: the *detection domain*.

Assume the source moves along the x-axis at constant speed v, and crosses the origin at the midpoint of a time interval of length t, during which the signal is collected. Denoting vt by ℓ and at by α, the expected signal at a sensor located at (x, y) equals, from (1)

$$\frac{\alpha}{|y|\ell}\left\{\tan^{-1}\left(\frac{x+\frac{\ell}{2}}{|y|}\right) - \tan^{-1}\left(\frac{x-\frac{\ell}{2}}{|y|}\right)\right\}. \qquad (5)$$

Fig. 2 is a contour plot of (5), with $\ell = 1$, centered on the origin, and $\alpha = 1$, for $0 \leq x, y \leq 3$. Fig. 2 compasses the change in

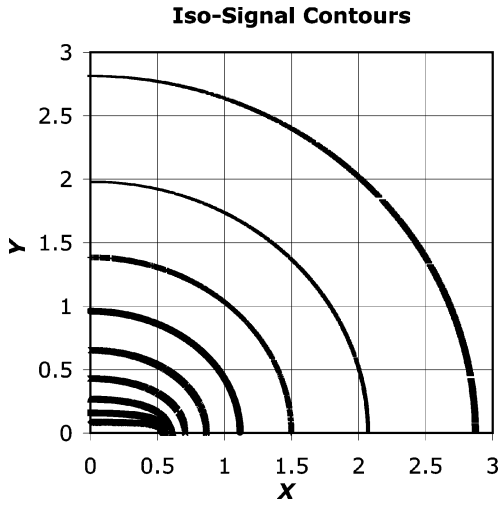

Fig. 2. Iso-signal contours for a moving source. A contour plot of (5), with $\ell = 1$ and $\alpha = 1$ for $0 \leq x, y \leq 3$. The contours depict loci where (5) evaluates to 32 (bottom left), 16, 8, 4, 2, 1, 1/2, 1/4, and 1/8 (top right), respectively.

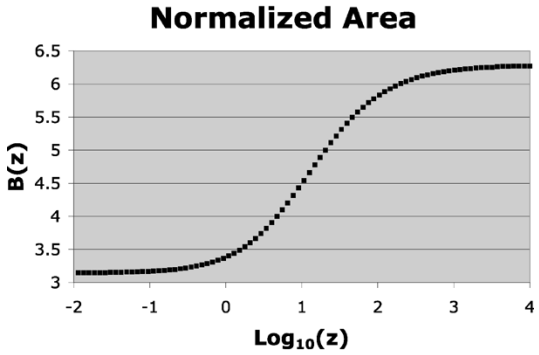

Fig. 3. $B(z)$. WOLOG $\ell = 1$. The normalized area $B(\Gamma/\alpha)$ $(= \mathcal{A}\Gamma/\alpha)$ of the portion of the xy plane where (5) exceeds Γ was determined by Monte Carlo simulation for various values of the ratio Γ/α. In detail, 10^8 points were uniformly sampled in the rectangle whose diagonal points were (0, 0) and $(\sqrt{\alpha/\Gamma} + 1/2, \sqrt{\alpha/\Gamma})$ because placing the sensor elsewhere in the first quadrant will yield a value of (5) less than Γ. The proportion of the points for which the expected signal exceeded Γ was multiplied by the area of this rectangle, by four and by Γ/α to yield the reported values for the function $B(z)$; *viz* (6). The abscissa is the logarithm base ten of z; $-2 \leq z \leq 4$. The ordinate is $B(z)$; $\pi \leq B(z) \leq 2\pi$.

shape of the domain from approximately linear (near field) to circular (far field).

Now consider the area $\mathcal{A}$ of the detection domain: the portion of the (x, y)-plane such that the signal, given by (5), exceeds a cutoff Γ. Scaling considerations yield

$$\mathcal{A} = \frac{\alpha}{\Gamma} B\left(\frac{\Gamma \ell^2}{\alpha}\right) \tag{6}$$

where $B(z)$ may be found, for instance, by determining the respective areas after arbitrarily fixing ℓ. Letting $\ell = 1$, these areas were estimated by Monte Carlo integration. $B(z)$ appears sigmoidal in the semilogrithmic Fig. 3.

Note that when $z < 10^{-2}$, $B(z) \doteq \pi$, and when $10^4 < z$, $B(z) \doteq 2\pi$, the limiting cases being the aforementioned circular and linear domains, respectively.

TABLE III
RATES OF "GETTING IT RIGHT" (TP, TN) FOR SOURCES OF DIFFERING AMPLITUDES USING DATA FROM 32 SENSORS. FOR THE TOP LINES, THE SENSORS ARE EQUALLY SPACED AND PLACED ALONG ONE OF THE 600-METER EDGES OF THE RECTANGLE. FOR THE MIDDLE LINES, THE SENSORS ARE EQUALLY SPACED WITH $x = 0$ AND $-5 \leq y \leq 5$. THE BOTTOM LINES, REPRODUCED FROM TABLE II, PERTAIN TO RANDOM PLACEMENT OF THE 32 SENSORS WITHIN THE ROADWAY. 1,000 DIFFERENT, UNIFORMLY DISTRIBUTED TRAJECTORIES (OF EACH CLASS) WERE SIMULATED AND THE MAXIMUM I_c WAS USED TO PREDICT THE CLASS, AS DESCRIBED IN THE METHODS

$a =$	1	10	100
TP	0.50	0.52	0.70
TN	0.50	0.57	0.87
TP	0.52	0.72	0.81
TN	0.50	0.95	0.99
TP	0.52	0.68	0.99
TN	0.50	0.89	1.00

In summary, the area of the detection domain, $\mathcal{A}$, is essentially, proportional to α/Γ. Due to the influence of $B(z)$, however, (with ℓ fixed) $\mathcal{A}$ can fall short of increasing as much as α/Γ, rendering the detection capabilities of a single sensor "less than linear" in α/Γ.

B. Simulations of DSN Detection

Many of our simulations concern the placement of DSN nodes uniformly and randomly inside the 10 m by 600 m rectangle modeling an inderdicted part of a road. We report estimates for TP and TN rates, recalling that the former denote the probability an incident source is inferred to be incident and the latter denote the probability a nonincident source is inferred to be nonincident. These rates appear in Tables I and II, and Table III presents analogous results for alternative node placements. To interpret these tables, note that over each 1-s interval of data collection, the expected number of signal counts at a detector at 1 m from the source equalled a and, with the exception of Table I, that the background rate equalled 10 s^{-1}[3].

Note, in Table II, the nonmonotonicity of the TP rates for $S = 10$. While this may partly be attributable to fluctuations in our simulations, it is also likely that the implemented node configuration is comparably effective at detecting sources with $a = 10$ as sources with $a = 31.25$ because nonmonotonicity persisted in more extensive simulations (data not shown).

In the vicinity of the top-right corner of Table II, it may be observed that decreases in a are compensable by reciprocal increases in S. Consider, however, $100 = aS$. As a decreases from ten to unity, there is a gradual decline of TP and a precipitous falloff of TN. Closer scrutiny of these cases is given in Table IV.

Thus, with $aS = 100$, reducing a usually results in smaller "signal" or smaller "signal to noise", the latter for the incident sources, and it therefore seems likely that the corresponding trends for the detection rates, exhibited in Table II, have veracity. These phenomena are featured in the conclusion.

To initiate investigations into the relationship between the complexity of "trajectory space" and the computational requirements of Bayesian methods, we determined how many sampled points were required to obtain convergence of the TP and TN

TABLE IV
HERE, $aS = 100$, SO THE RESPECTIVE VALUES OF S ARE 100, 32 AND 10. WITH T STANDING EITHER FOR TP OR TN, E_{T} DENOTES THE RESPECTIVE AVERAGE OF $(\log I_1 - \log I_2)/(\log I_1 + \log I_2)$ AND σ_{T} IS THE CORRESPONDING STANDARD DEVIATION

$a =$	1.0	3.125	10.0
E_{TP}	7×10^{-4}	5×10^{-4}	3×10^{-3}
σ_{TP}	1×10^{-2}	3×10^{-3}	2×10^{-2}
E_{TN}	-2×10^{-6}	-8×10^{-6}	-3×10^{-5}
σ_{TN}	3×10^{-6}	1×10^{-5}	4×10^{-5}

rates, to within about 1% of the asymptotic values, for ensembles of trajectories of varying complexities and for networks with 10 nodes, i.e., $S = 10$. For the foregoing parameter spaces, the respective $p = 10^4$.

Simplified spaces were obtained by taking all speeds equal 20 m/s (the average in the foregoing simulations). Comparable accuracy of the rates was achieved by $p \doteq 10^4$.

"Complexified" spaces were obtained by giving incident sources both x *and* y components of velocity, with the former being positive and with the magnitude of the velocity distributed uniformly between 10 and 30 m/s, as before. Encounters with the top and bottom (600 m) edges resulted in elastic collisions: reversing the y-component of velocity. Nonincident sources moved parallel to the axis of the roadway, as before. Only a modestly greater p was required for achieving comparable accuracy: $p \doteq 10^5$ sufficed for obtaining the comparable level of accuracy.

For $a = 100$, in the last case the corresponding TP rate was 0.75; Table II gives 0.83 for the analogous case where the velocity is parallel to the x-axis. For the simplified ensembles with only one speed, the corresponding TP rate was 0.88. (The respective TN rates were essentially identical.)

We also simulated alternative node configurations, all with $S = 32$. One of these configurations had a uniform placement of its nodes along one of the long edges of the rectangular domain. Deployment on the "shoulder" has its practical advantages; deployment within the roadway awaits, among other things, further miniaturization. The other new configuration had the nodes uniformly spaced along the y axis, transverse to the roadway—our (flat) caricature of a midsection portal monitor. It should be noted that a fair proportion of trajectories in V_1 do not pass through the portal, as the parameter space was not designed as a test for them. TP and TN rates are compared with the rates given in Table II for uniform, random placement of the same number of nodes within the rectangular domain. For convenience, these rates are duplicated in Table III.

Finally, we investigated the effects of changing the background rate. These simulations had 32 sensors, randomly placed in the roadway. Results are given in Table I. It appears that S must exceed 32 in order to leverage reductions in b, when a is small.

IV. CONCLUSION

Based on our results, implementation of Bayesian methods on sensor networks may be profitable [11]. Furthermore, analogues of the observed phenomena, such as the nonscalability of performance, should occur elsewhere [5].

Simulation is effective for evaluating candidate node placements [*viz* Table III]. For example, one may readily detect sources of amplitude 31.25 counts s^{-1}, moving at constant velocity of magnitude between 10 and 30 $\mathrm{m\ s}^{-1}$, when background equals 10 counts s^{-1}, using 100 randomly placed sensors in a 6,000 m^2 section of roadway. Placement on the "shoulder" was much less effective.

To illustrate the implications of our results for interdiction, consider, for instance, a teletherapy unit used for treating cancer, such as the Theratron Equinox with its full complement of Cobalt-60 [1]. With its intrinsic shielding and in its "off" mode, its radiation, at 1 m, is not more than 2 mrem (0.2 Sv) /min [12]. The latter is about 60 times background [300 mrem (30 Sv) /yr] [13], and mobile sources emitting such signals should be detectable by a 10-node, in-roadway DSN, based on our simulations with $a = 312.5$ and a background of 10 counts s^{-1} [*viz* Table II], subject, however, to the following caveats. Increasing the number of nodes could be appropriate for other background rates (cf. Table I). In addition, the signal would plainly be weaker for a source above the roadway than those modeled herein—at road level. The effects of a substantial reduction of the prior probability for incidence should be modest, as is characteristic of orthodox Bayesian methods. Other configurations, such as the portal-like configuration of Table III, could be equally advantageous for this application.

From (6), the area under surveillance by a sensor is, to a first approximation, proportional to a, with all else fixed [*viz* (6)], and the average total area under surveillance by the DSN is approximately proportional to aS. From Table II, we find empirically that for $\sqrt{S}/a \tilde{<} 6$ the detection rates essentially depend only on the product aS, as one may ascertain from the respective "off diagonals" of Table II, but otherwise, they depart from this simple dependence (cf. [5]). One might attempt rationalization of the latter phenomena with the a-dependent "morphing" of sensor's detection domains, depicted in Fig. 2.

Consider, for example, (6) with $a = 10$ and $S = 10$ versus $a = 1$ and $S = 100$. With $t = 1$, $\alpha = 1$ and $\Gamma = 10 \sim b$ and $\ell = 20$ m (its average value), from (6), the area $\mathcal{A}$ "under surveillance" by each sensor is about 6/10 m^2 ($z = \Gamma\ell^2/\alpha \doteq 4000$). In both cases, less than 1% of the area of the domain of incidence is under surveillance by precisely one sensor, and less than 0.01% by more than one sensor, implying that the "areal predictions" for one sensor should extend to the network. Furthermore, 100 sensors with $a = 1$ should jointly have greater area under surveillance than 10 sensors with $a = 10$, and it follows that the first sensor net should have correspondingly increased TP rate, at odds with our results.

Our recourse is in stochasticity. Near the detection limit, the latter phenomena must reflect the chance occurrence of data mimicking that of a source. Attention may focus on signal-to-background considerations, as this underlies detection. Let a decrease and let $S \propto a^{-1}$. Although the expected number of sensors receiving an above-cutoff signal would remain the same, the number of "other lines" of sensors – receiving background alone – would increase $\propto a^{-1}$. The implication is that an effective cutoff for detection must be raised as a decreases. Based on Gaussian statistics, this cutoff $\propto \sqrt{\log S}$. Although this dependence is weak, it nevertheless could suffice, in the range

$10 \leq S \leq 320$, for rationalizing the observed departures from aS-dependence. This hypothesis yields the prediction that, for all values of aS, decreases in a are, ultimately, not compensable by reciprocal increases in S. Our data are not extensive enough to distinguish between the previously employed $\sqrt{S}$ dependence and this $\sqrt{\log S}$ dependence. It would be useful to clarify the situation and, thereby, to be able to predict analogous behavior for more complicated universes of trajectories. The nonscaling should be much more apparent for sensor networks deployed with three dimensions.

The computational requirements of the Bayesian methods have been shown to be appreciable but not prohibitive. Unlike the estimation of the parameters of a radioactive source, for which the runtime scales exponentially in the number of parameters [3], for detection, it is a boon that realistic source parameter spaces appear to be amenable to Bayesian methods because real-world problems involve more complexity than modeled herein. The intrinsic difficulty of detection seems to increase with this complexity [5] – a topic worthy of theoretical investigation.

For our relatively uncomplicated parameter spaces, in five CPU seconds, 20 seconds' worth (20 time intervals) of data from ten nodes were analyzed, with negligible memory requirements. Thus, for modest S, minimal improvements will be required to implement them on the bare-bones processors typically accorded DSN nodes, in order to achieve Bayesian detection in real time. For instance, quasi Monte Carlo methods offer comparable accuracy of integration with reduced computational overhead [3], [14].

Although it sufficed to address many issues empirically herein, additional challenges for theoreticians remain. It would be useful, for example, to predict the "fluctuations in classification" as a function of the extent of sampling of parameter space: predictions germane to statistical properties of estimates for I_1/I_2 [*viz* Fig. 1]. A more ambitious aim would be an asymptotic upper bound on the Bayesian methodology's effectual runtime, applicable when the number of nodes increases indefinitely: extrapolating from the observed approximately quadratic dependence on the number of nodes.

In practice, most of the nodes' data are no more than noise, and, for efficiency, one should seek ways to adaptively discover profitable subsets of nodes for the Bayesian computation. Markov chain Monte Carlo might be useful for constructing subsets of fixed size which maximize $\Pr(\text{data})$, and detection could be based on the running-average maximum probability. This approach might, by curtailing noise, improve the detection rates over those based on analyzing the data from all the nodes, as pursued herein—without significantly degrading the detection rates. Precedent exists in the efficacious detection of sources with known trajectories [3].

APPENDIX
INTEGRAL OF EXPECTED SIGNAL AMPLITUDE

The expected instantaneous rate of signal acquisition is assumed to be inversely proportional to the distance squared from the source, i.e., detection is assumed to be isotropic [3]. Then, when the relative velocity between the source and the node is constant, the following integral, multiplied by the amplitude of the source (with dimensions $\mathrm{m}^2\mathrm{s}^{-1}$) equals the expected signal (the expected number of signal counts) collected by a sensor between times 0 and t (> 0):

$$I(\mathbf{u},\mathbf{v};t) \stackrel{\text{def}}{=} \int_0^t \frac{dt'}{(\mathbf{v}t'+\mathbf{u})^2} = \int_0^t \frac{dt'}{(\mathbf{v}\cdot\mathbf{v})t'^2+2(\mathbf{u}\cdot\mathbf{v})t'+\mathbf{u}\cdot\mathbf{u}}$$

where $\mathbf{u}$ denotes the difference between source and sensor coordinates, at time 0, and with $\mathbf{v}$ denoting the difference between the source and sensor velocities (assumed constant between 0 and t). Here, $\mathbf{u} \neq 0$ (because, otherwise, the integral is infinite). Two cases present themselves: i) $\|\mathbf{v}\| = 0$ (with $\|\mathbf{v}\|$ denoting the Euclidean norm of $\mathbf{v}$) and ii) otherwise.

i) $I(\mathbf{u},\mathbf{v};t) = t/\|\mathbf{u}\|^2$.

i.a) Here, if $\|\mathbf{u}\|^2\|\mathbf{v}\|^2 = (\mathbf{u}\cdot\mathbf{v})^2$, i.e., $\mathbf{u} = \gamma\mathbf{v}$ with $\gamma \neq 0$, then

$$I(\mathbf{u},\mathbf{v};t) = \begin{cases} \infty & -t \leq \gamma \leq 0, \\ \frac{t}{(\gamma(t+\gamma)\|\mathbf{v}\|^2)}, & \text{otherwise.} \end{cases}$$

ii.b) Alternatively, i.e., $\|\mathbf{u}\|^2\|\mathbf{v}\|^2 \neq (\mathbf{u}\cdot\mathbf{v})^2$, "completing the square" readily yields

$$I(\mathbf{u},\mathbf{v};t) = \beta\left(\tan^{-1}\{\beta(\|\mathbf{v}\|^2 t + (\mathbf{u}\cdot\mathbf{v}))\} - \tan^{-1}\{\beta(\mathbf{u}\cdot\mathbf{v})\}\right) \tag{7}$$

where the range of the arctangents is $[-\pi/2, \pi/2]$, and where

$$\beta \stackrel{\text{def}}{=} \frac{1}{\sqrt{\|\mathbf{u}\|^2\|\mathbf{v}\|^2 - (\mathbf{u}\cdot\mathbf{v})^2}}$$

with $\beta > 0$. Herein, (7) is the case of interest.

ACKNOWLEDGMENT

The authors are indebted to R. Nemzek and T. Warnock, Los Alamos National Laboratory, for sharing their expertise, and to G. Sandine, LA Computers (laclinux.com), for providing access to the (dual-opteron) computer on which most of the simulations were performed. The U.S. government has rights to use, reproduce, and distribute this information. The public may copy and use publicly released information without charge, provided that this notice and any statement of authorship are reproduced on all copies. Neither the government nor the university makes any warranty, express or implied, or assumes any liability or responsibility for the use of this information.

REFERENCES

[1] A. Oppenheimer. (2004, Sep.) The radiological threat widens. *Jane's Terrorism & Security Monitor.* [Online] Available: http://www.janes.com/security/international_security/news/jtsm/jtsm0 40909_1_n.shtml

[2] S. Brennan, A. Mielke, D. Torney, and B. Maccabe, "Radiation detection with distributed sensor networks," *Comput.*, vol. 37, pp. 57–59, 2004.

[3] R. J. Nemzek, J. S. Dreicer, D. C. Torney, and T. T. Warnock, "Distributed sensor networks for detection of mobile radioactive sources," *IEEE Trans. Nucl. Sci.*, vol. 51, no. 4, pp. 1693–1700, Aug. 2004.

[4] R. Nishiura, T. Oka, H. Fujiwara, Y. Tsutaka, S. Yasue, H. Nakumura, and Y. Matsuoka, "Inverse problem for distribution of radioactive source using the SPM method," in *Proc. Inverse Problems Engineering Mechanics Int. Symp.*, M. Tanaka and G. S. Dulikravich, Eds., Berlin, Germany, 1998, pp. 467–474.

[5] D. L. Stephens and A. J. Peurrung, "Detection of moving radioactive sources using sensor networks," *IEEE Trans. Nucl. Sci.*, vol. 51, no. 5, pp. 2273–2278, Oct. 2004.

[6] J. O. Berger and D. A. Berry, "Statistical analysis and the illusion of objectivity," *Amer. Scientist*, vol. 76, pp. 159–165, 1988.

[7] X.-Y. Song and S.-Y. Lee, "A Bayesian model selection method with applications," *Comput. Statist. Data Anal.*, vol. 40, pp. 539–557, 2002.
[8] R. Y. Rubinstein, *Simulation and the Monte Carlo Method*. New York: Wiley, 1981.
[9] G. A. Mikhailov, "Monte-Carlo method," in *Encyclopædia of Mathematics*, M. Hazewinkel, Ed. Dordrecht, The Netherlands: Kluwer, 1990, vol. 6, pp. 308–311.
[10] W. H. Press, *Numerical Recipes in Fortran 77: The Art of Scientific Computing*. Cambridge, U.K.: Cambridge Univ. Press, 1992.
[11] A. M. Jorgensen, "A Bayesian Approach to Nuclear Detection and Characterization in a DSN-CC," Los Alamos National Laboratory, Los Alamos, NM, Tech. Rep. 03–2590, 2003.
[12] D. Aikenhead, private communication, Dec. 2004.
[13] M. Eisenbud, "Environmental radioactivity," in *Encyclopedia of Physical Science and Technology*. San Diego, CA: Academic, 1992, vol. 6, p. 220.
[14] H. Neiderreiter, *Random Number Generation and Quasi-Monte Carlo Methods*. Philadelphia, PA: SIAM, 1992.